The Cryosphere Discuss., 9, 301–331, 2015
www.the-cryosphere-discuss.net/9/301/2015/
doi:10.5194/tcd-9-301-2015

The Cryosphere Discussions
Open Access

A 3-D simulation of drifting snow in the turbulent boundary layer

N. Huang[1,2] **and Z. Wang**[1,2]

[1]Key Laboratory of Mechanics on Disaster and Environment in Western China (Lanzhou University), The Ministry of Education of China, Lanzhou, 730000, China
[2]Department of Mechanics, School of Civil Engineering and Mechanics, Lanzhou University, Lanzhou, 730000, China

Received: 10 November 2014 – Accepted: 16 December 2014 – Published: 15 January 2015

Correspondence to: Z. Wang (wangzhsh2013@lzu.edu.cn)

Published by Copernicus Publications on behalf of the European Geosciences Union.

Abstract

The drifting snow is one of the most important factors that affect the global ice mass balance and hydrological balance. Current models of drifting snow are usually one- or two-dimensional, focusing on the macroscopic quantities of drifting snow under temporal average flow. In this paper, we take the coupling effects between wind and snow particles into account and present a 3-D model of drifting snow with mixed grain size in the turbulent boundary layer. The Large Eddy Simulation (LES) method is used for simulating the turbulent boundary layer of the wind field and the 3-D trajectory of every motion snow particle is calculated through Lagrangian Particle Tracking method. The results indicated that the drifting snow in the turbulent boundary layer has apparent 3-D structure and snow streamers, which lead to an intermittent transport of the snow particles and spatial inhomogeneity, and the motion trajectories of snow particles, especially the small snow particles, are obviously affected by the turbulent fluctuation. The macro statistics of drifting snow indicates that the spanwise velocity of snow particles increases with height and is one order smaller than that of streamwise velocity. Furthermore, the diameter distribution of snow particles in the air along the height shows a stratification structure.

1 Introduction

The phenomenon of the loose snow particles traveling near the land surface under the action of wind is known as drifting snow. As a typical two-phase flow, drifting snow is widely distributed in the globe and has significant impacts on the natural environment and the social economy. On one hand, drifting snow is one of the main causes of the temporal and spatial variation of snow distribution, contributes greatly to the mass balance of the Antarctic ice sheets, and further affects global climate system. The seasonal snow cover also deeply affects the hydrological balance in cold regions, thus is of glaciological and hydrological importance. On the other hand, drifting snow causes

TCD
9, 301–331, 2015

snow accumulation on the road and reduces visibility, which may seriously affect the traffic and human activities, and its resultant non-uniform distribution of snow layer may induce and aggravate various natural disasters, such as flood, avalanche, mudslides and landslide (Michaux et al., 2002). These disasters may result in not only huge direct and indirect economic losses, but also human casualties. Thus, in-depth study on the drifting snow is considered to be essential to comprehensively understanding the ice mass balance and hydrological balance.

The transport processes of snow grains have been extensively investigated (Pomeroy et al., 1993; Lehning et al., 2002; Bavay et al., 2009). Many models were proposed by taking the snow particles as continuous phase (Uematsu et al., 1993; Mann, 2000; Taylor, 1998; Déry and Yau, 1999; Fukushima et al., 1999, 2001; Xiao et al., 2000; Bintanja, 2000a, b). Obviously, the above assumption is not in agreement with the real situation. In addition, these models could reveal neither the movement mechanisms of snow particles nor the factors affecting the behaviors of snow particles. Recently, Nemoto and Nishimura (2004) studied the snow drifting process based on particle tracking in a turbulent boundary layer and their 1-D model included four sub-processes: the aerodynamic entrainment of snow grains, grain-bed collision, grain trajectories and wind modification. Later, Zhang and Huang (2008) presented a steady state snow drift model combined with the initial velocity distribution function and analyzed the structure of drifting snow at steady state. However, neither the details of the spatial variation of snow drifting nor the whole turbulent structure of wind field can be described due to limitation of their models. Furthermore, snow particles were uniform size in most previous models, which is different from the natural situation. To date, a comprehensive study on drifting snow in the turbulent field is indispensable for a thorough understanding of the complex drifting snow.

In this paper, we present a physical 3-D numerical model for drifting snow in the turbulent boundary layer based on the LES of Advanced Regional Prediction System (ARPS, version 5.3.3) by taking the 3-D motion trajectory of snow particles with mixed grain size, the grain-bed interaction, and the coupling effect between snow particles and

TCD
9, 301–331, 2015

wind field into consideration and used it to directly calculate the velocity and position of every single snow particle in turbulent atmosphere boundary layer, the transport rate and velocity distribution characteristics of drifting snow, and the mean particles size at different heights. The paper is structured as follows: Sect. 2 briefly introduces the model and methods; Sect. 3 presents the simulation results and discussions, and Sect. 4 is the conclusion.

2 Model and methods

2.1 Turbulent boundary layer

The ARPS developed by University of Oklahoma is a three-dimensional, non-hydrostatic, compressible LES model and has been used for simulating wind soil erosion (Vinkovic et al., 2006; Dupont et al., 2013). In this paper, it is used for modeling the drifting snow.

Snow saltation movement in the air is a typical two-phase movement, in which the coupling of particles and the wind field is a key issue. The conservation equations of momentum and subgrid scale (SGS) turbulent kinetic energy (TKE) after filtering with considering the impact of the presence of particles on the flow field can be expressed as (Vinkovic et al., 2006; Dupont et al., 2013):

$$\frac{\partial \widetilde{u}_i}{\partial t} + \widetilde{u}_j \frac{\partial u_i}{\partial x_j} = -\frac{1}{\overline{\rho}} \frac{\partial}{\partial x_i} \left(\widetilde{p}'' - \alpha_{\mathrm{div}} \frac{\partial \overline{\rho} \widetilde{u}_j}{\partial x_i} \right) - g \left(\frac{\widetilde{\theta}''}{\overline{\theta}} - \frac{c_p}{c_v} \frac{\widetilde{p}''}{\overline{p}} \right) \delta_{i3} - \frac{\partial \tau_{ij}}{\partial x_j} - f_i \tag{1}$$

$$\frac{\partial e}{\partial t} + \widetilde{u}_j \frac{\partial e}{\partial x_j} = -\tau_{ij} \frac{\partial \widetilde{u}_i}{\partial x_j} + \frac{\partial}{\partial x_j} \left(2 \left(\left(1 - \delta_{j3}\right) \nu_{\mathrm{th}} + \delta_{j3} \nu_{\mathrm{tv}} \right) \frac{\partial e}{\partial x_j} \right) - \frac{g}{\overline{\theta}} \tau_{3\theta} - \varepsilon - \frac{1}{V_{\mathrm{grid}}} \sum_{s=1}^{N_{\mathrm{p}}} \frac{m_{\mathrm{p}}}{\overline{\rho}} \frac{2e}{T_{\mathrm{p}} + T_{\mathrm{L}}} f\left(Re_{\mathrm{p}}\right) \tag{2}$$

TCD
9, 301–331, 2015

where the tilde symbol indicates the filtered variables and the line symbol represents grid volume-averaged variables. $x_i (i = 1,2,3)$ stand for the streamwise, lateral, and vertical directions, respectively, u_i refers to the instantaneous velocity component of three directions, δ_{ij} is the Kronecker symbol, α_{div} means the damping coefficient, p and ρ are the pressure and density of air, respectively; g is the gravity acceleration, θ indicates the potential temperature, c_p and c_v are the specific heat of air at constant pressure and volume, respectively; t is time, τ_{ij} denotes the subgrid stress tensor, and f_i is the drag force caused by the particles and can be written as (Yamamoto et al., 2001):

$$f_i = \frac{1}{\rho V_{\mathrm{grid}}} \sum_{s=1}^{N_{\mathrm{p}}} m_{\mathrm{p}} \frac{u_i(x_{\mathrm{p}}(t),t) - u_{\mathrm{p}i}(t)}{T_{\mathrm{p}}} f(Re_{\mathrm{p}}) \tag{3}$$

where V_{grid} is the grid cell volume, N_{p} stands for the number of particles per grid, m_{p} means the mass of particles, $u_{\mathrm{p}i}(t)$ and $u_i(x_{\mathrm{p}}(t),t)$ represent the velocity of particles and the wind velocity at grain location at time t, respectively, and $f(Re_{\mathrm{p}})$ is an empirical relation of the particle Reynolds number Re_{p} (Clift et al., 1978):

$$\begin{aligned} f(Re_{\mathrm{p}}) &= 1 \qquad\qquad (Re_{\mathrm{p}} < 1) \\ f(Re_{\mathrm{p}}) &= 1 + 0.15 Re_{\mathrm{p}}^{0.687} \quad (Re_{\mathrm{p}} \geq 1). \end{aligned} \tag{4}$$

In the Eq. (2), e is the SGS TKE, v_{th} and v_{tv} stand for the horizontal and vertical eddy viscosities, respectively, $\tau_{3\theta}$ is the subgrid heat flux, and ε indicates the dissipation rate of SGS TKE. T_{p} and T_{L} represent the particle response time and the Lagrangian correlation timescale, respectively, and can expressed as

$$T_{\mathrm{p}} = \frac{\rho_{\mathrm{p}} d_{\mathrm{p}}^2}{18\rho\nu} \quad \text{and} \quad T_{\mathrm{L}} = \frac{4e}{3C_0\varepsilon} \tag{5}$$

where C_0 is the Lagrangian constant and ν denotes the molecular kinematic viscosity.

TCD
9, 301–331, 2015

2.2 Governing equation of particle motion

Because snow particles have much higher density ρ_p than air ($\rho_p/\rho \approx 10^3$) and much smaller diameter d_p than Kolmogorov scale, in our simulation, they are approximately regarded as a sphere and only possess gravity and drag force. Thus, their motion governing equation can be expressed as (Vinkovic et al., 2006)

$$\frac{\mathrm{d}\boldsymbol{x}_p(t)}{\mathrm{d}t} = \boldsymbol{v}_p(t) \tag{6}$$

$$\frac{\mathrm{d}\boldsymbol{v}_p(t)}{\mathrm{d}t} = \frac{\boldsymbol{v}(\boldsymbol{x}_p(t),t) - \boldsymbol{v}_p(t)}{T_p} f(Re_p) + \boldsymbol{g} \tag{7}$$

where $\boldsymbol{v}_p(t)$ and $\boldsymbol{v}(\boldsymbol{x}_p(t),t)$ are the velocity of the particle and the fluid velocity of particle position at time t, respectively.

It is worth noting that the inertia effect of snow particles is considered by evaluating the maximum particle response time, so the particle motion is the dynamical calculation of time step, which is guaranteed to be less than the maximum particle response time.

2.3 Rebound and splash

The collision of saltating particles with the bed surface is a key physical process in saltation, as it will rebound with a certain probability and may splash new saltating particles into the air (Shao and Lu, 2000). Kok and Renno (2009) have proposed a physical splashing function based on the conservation of energy and momentum. Thus, the saltation process under various physical environments can be accurately simulated and applied to the mixed soils and drifting snow.

2.3.1 Rebounding

The grain-bed interaction is a stochastic process, in which the impact particles may rebound with a certain probability. If a particle rebounds into the air, it can be described

TCD
9, 301–331, 2015

using three variables: the velocity v_{reb}, the angle toward the surface α_{reb} and the angle toward a vertical plane in the streamwise direction β_{reb}.

The rebound probability can be expressed as:

$$P_{reb} = B[1 - \exp(-\gamma v_{imp})] \quad (8)$$

where v_{imp} is the impact velocity of particle, B and γ are the experienced parameters. Here, $B = 0.95$ and $\gamma = 2\,\mathrm{s\,m^{-1}}$ are employed.

For the velocity after rebound v_{reb}, Kok and Renno (2009) indicate that the fraction of kinetic energy retained by the rebounding particle approximately follows normal distribution as follow:

$$v_{reb}^2 = ((45 \pm 22)\,\%) v_{imp}^2. \quad (9)$$

Two angles are introduced in the rebound process to describe the rebound direction as mentioned above. The angle α_{reb} approximately follows an exponential distribution. Although it is not affected by the impact velocity, it decreases exponentially with the increase of particle diameter (Rice et al., 1995; Zhou et al., 2006). The relationship of average value of rebound angle to particle diameter can be expressed as:

$$\langle \alpha_{reb} \rangle = 161.46 e^{-\frac{d_p}{250}} + 0.15 \quad (10)$$

where d_p is measured in the unit of micrometer. However, the angle β_{reb} was rarely involved in previous studies and may not strongly affect the saltation process (Dupont et al., 2013). Here we choose $\beta_{reb} = 0^\circ \pm 15^\circ$.

2.3.2 Splashing

The newly ejected particles and the "dead particles" (not rebounded) will reach equilibrium when the saltation process becomes stable.

TCD
9, 301–331, 2015

The number of newly ejected particles is usually proportional to the impact velocity and can be written as (Kok and Renno, 2009):

$$N = \frac{a}{\sqrt{gD}} \frac{m_{\text{imp}}}{\langle m_{ej} \rangle} v_{\text{imp}} \tag{11}$$

where a is a dimensionless constant in the range of 0.01– 0.05 (here $a = 0.03$), D is the typical particle size ($\langle d_{\text{p}} \rangle$ in this paper), m_{imp} is the mass of impacting particle and $\langle m_{ej} \rangle$ is the average mass of ejection grains.

Once a new particle is splashed into the air, it can also be characterized by its velocity v_{ej}, its angle toward the surface α_{ej} and its angle toward a vertical plane in the streamwise direction β_{ej}.

The speed of the ejected particles is exponentially distributed. Kok and Renno (2009) developed a physical expression of the average dimensionless speed of the ejected particle as follow:

$$\frac{\langle v_{ej} \rangle}{\sqrt{gD}} = \frac{\langle \lambda_{ej} \rangle}{a} \left[1 - \exp\left(- \frac{v_{\text{imp}}}{40\sqrt{gD}} \right) \right] \tag{12}$$

where $\langle \lambda_{ej} \rangle$ is the average fraction of impacting momentum applied on the ejecting surface grains. We choose $\langle \lambda_{ej} \rangle = 0.15$ in this paper.

Kok and Renno (2009) indicated that the angle α_{ej} approximately follows an exponential distribution and its mean value is 50°. In addition, the angle $\beta_{ej} = 0° \pm 15°$.

2.4 Simulation details

The blowing snow process in the turbulent boundary layer is simulated and the simulation results are compared with the existent experiment results. Computational region is set as 4 m × 1.2 m × 1.4 m and divided into two sections, as show in Fig. 1. The first zone is the fully developed wind field region with a steady turbulent boundary layer

TCD
9, 301–331, 2015

extending from $x = 0\,\mathrm{m}$ to $x = 2\,\mathrm{m}$ and a flow field cycle at $x = 1\,\mathrm{m}$. The second zone is the snow blowing region from $x = 2\,\mathrm{m}$ to $x = 4\,\mathrm{m}$, where a sufficient loose snow layer is set on the ground.

In this model, the grid has a uniform size of $\Delta x = \Delta y = 0.02\,\mathrm{m}$ in the horizontal direction, and the average mesh size of $\Delta z = 0.02\,\mathrm{m}$ in the vertical direction. The grid is stretched by cubic function to acquire more detailed information of the surface layer and the smallest grid is $\Delta z_{\min} = 0.002\,\mathrm{m}$.

A turbulent boundary layer over a snow bed is generated using the dynamic Smagorinsky–Germano subgrid-scale (SGS) model by setting the soil type, reasonable roughness and an initial field with turbulent fluctuations. For the flow field, we applied the rigid ground boundary condition at the bottom, the open radiation boundary in the top, the periodic boundary condition in the spanwise direction, the open radiation boundary condition at the end of the domain along the streamwise direction and the periodic boundary condition in the inflow with the cycle location at $x = 1.0\,\mathrm{m}$. The initial wind database is obtained from the experimental results of wind tunnel. The snow particles have circulatory motion in the lateral boundary.

The size distribution of snow particles in this paper is fitted to the experiment results obtained from field observations of SPC (Schmidt, 1984), that is

$$f(d_\mathrm{p}) = \frac{d_\mathrm{p}^{(\alpha-1)}}{\beta^\alpha \Gamma(\alpha)} \exp(-d_\mathrm{p}/\beta) \tag{13}$$

where α and β are the shape and scale parameters of gamma-function distribution, respectively. Here, the diameters of 2617 snow particles are counted and their distribution is presented in Fig. 2. The mean diameter is $\langle d_\mathrm{p} \rangle = 350\,\mu\mathrm{m}$. The results are in consistence with those observational results of the natural snow (Omiya et al., 2011).

The density of snow particles and air are 912 and $1.225\,\mathrm{kg\,m^{-3}}$, respectively. And the surface roughness and the molecular kinematic viscosity of snow particles are $z_0 = \langle d_\mathrm{p} \rangle / 30$ and $\nu = 1.5 \times 10^{-5}$, respectively. Several particles will be forced to take off

TCD
9, 301–331, 2015

from bed surface with random velocities ($u_{pi} = (0 \sim 1)\,m\,s^{-1}$) at random positions in the domain at the initial moment of drifting snow.

The processes of snow blowing with the wind velocity of $U_e = 4 \sim 10\,m\,s^{-1}$ are performed at environmental temperature of $-10\,^{\circ}C$ and initial relative humidity of 90 %.

3 Results and discussions

3.1 Analysis of the flow field

Almost all the flows at atmospheric boundary layer are turbulent. Therefore, the simulation of turbulent boundary layer is the key and basis for accurately simulating the drifting snow. Enough time is supplied for forming a stable turbulent boundary layer before particles taking off. The computational region is relative small and the inflow contains the real turbulent fluctuation.

Figure 3 shows the cloud map of velocity along the streamwise direction ($U_e = 7\,m\,s^{-1}$) (a) before the snow particles take off ($t = 5\,s$) and (b) when the drifting snow has been sufficiently developed ($t = 20\,s$). The slice elicited by arrows displays the velocity cloud map of U direction at height $H = 0.001\,m$. Figure 3a-1 and a-2 shows the contour surface map ($\pm 0.5\,m\,s^{-1}$) of wind velocity along spanwise direction and vertical direction, respectively, at time $t = 5\,s$, and Fig. 3b-1 and b-2 shows the corresponding results at time $t = 20\,s$.

It can be observed from Fig. 3 that homogeneous turbulent fluctuations are distributed in the fully developed boundary layer. When the stable drifting snow is formed, the wind velocity will significantly decrease in the drifting snow region due to the reaction force of the snow particle and the turbulent fluctuations gradually become non-uniform in the drifting snow region. This is mainly due to the presence of the snow streamers-resulted great difference in the number concentration of snow particles at different positions (details are shown in Sect. 3.2).

TCD
9, 301–331, 2015

In addition to the turbulent fluctuation, the wind profile can also be obtained by the time averaging and spatial averaging of a time-series of wind velocities ($t = 3 \sim 5$ s and the time interval is 0.01 s). As shown in Fig. 4, the method leads to similar wind profiles to that of wind tunnel experiment at different wind speeds.

When the turbulent boundary layer is fully developed, the snow particles will be released and the motion feature of snow particles could be further obtained.

3.2 Snow streamers

The saltation process, either in the field or in the wind tunnel, exhibits a temporospatial discontinuity. This discontinuity is affected by many factors such as turbulent fluctuation, topography, surface moisture, roughness elements, etc. (Stout and Zobeck, 1997; Durán et al., 2011). Different from previous models which are unable to clearly describe the drifting snow structure, our 3-D model could be used to directly calculate the 3-D trajectory of every snow particle and further intuitively demonstrate the overall structure of snow saltation layers because it describes the macroscopic performance of a large amount of drifting snow particles.

Figure 5a and b shows the typical trajectories of snow particles with diameter of 100 and 300 µm, respectively, in which the blue dotted line denotes the motion trajectory that is not affected by the turbulence. It can be seen that turbulence can significantly affect the trajectories of snow particles with diameter smaller than 100 µm, and may drive snow particles with diameter of 100 µm moving 5–6 m during one saltation process. By contrast, the trajectories of larger snow particles are less affected by the turbulent fluctuation, showing only slight influence on the saltation height, saltation distance and landing position of snow particles.

A large amount of snow particles move complexly in the turbulent boundary layer, constituting the overall structure of the drifting snow. Figure 6 shows the top view of the snow-driving particles concentration and the horizontal cloud map of streamwise wind velocity at corresponding moment, in which, (a) and (b) represent the moment of $t = 8$ s and $t = 12$ s, respectively.

TCD
9, 301–331, 2015

It can be observed from Fig. 6 that snow streamers with high saltating particle concentration obviously swing forward along the downwind direction, merging or bifurcating during the movement. It can also be found that the snow streamers with elongated shape differ greatly in length, but only 0.1–0.2 m in width. From the corresponding slices of wind velocity cloud map, it can be seen that many low-speed streaks exist in the near-wall region of the turbulent boundary layer. By comparing the concentration and corresponding velocity cloud map, it can be found that the particle concentration shows a direct proportional relationship with the local wind velocity, that is, only few snow particles present in the low-speed streaks.

The in-homogeneous take off and splash of the snow particles in the turbulent wind field are the main reasons for the formation of snow streamers. The shape and size of streamers largely depend on the flow structure of the turbulent boundary layer. In addition, during the full development of drifting snow, the saltating particles and wind field are in the state of dynamic balance due to the feedback effect of each other. When the number concentration of snow particles at a certain position is high enough, the local wind velocity will be significantly reduced, resulting in a lower splash level. Thus the streamer will gradually weaken or even disappear. In contrast, the local wind speed in the low concentration region will increase, which enhances the splash process, so the snow particles will grow rapidly and form a streamer. Furthermore, the fluctuating velocity may also change the movement direction of snow particles. All the above reasons together cause the serpentine forward of the snow streamers.

3.3 Snow transport rate

Snow transport rate (STR) is one of the most important indicators of the strength of the drifting snow. In this simulation, the snow particles will be collected if they pass through the section located at $x = 3$ m during the time of $t = 10$–20 s. Figure 7a shows the time evolution of STR per width in different friction wind velocity. It can be seen that the STR per width increases rapidly and reaches a dynamic equilibrium state in a short time. With the friction wind speed increasing, the time needed to reach the equilibrium state

TCD
9, 301–331, 2015

also increases. During the transport process, STR per width also slightly fluctuates and its fluctuation amplitude is proportional to the friction wind velocity, mainly owing to the intermittent behavior of drifting snow. At the same time, it can be observed from Fig. 7b that the STR per width increases with friction wind velocity increasing, in consistence with the existing experiment results.

The average particle concentrations under different friction wind velocities as a function of height are shown in Fig. 8a. It is clear from the figure that the average particle concentrations at different friction wind velocity similarly fluctuate with height, that is, they decrease with height increasing. And the greater the friction wind velocity, the greater the maximum height the snow particles can achieve. Further analysis shows that the difference of average particle concentrations under different friction wind speed is proportional to height. For example, at the height of 0.001 m, the average particle concentration at friction wind velocity of $u_* = 0.361\,\mathrm{m\,s^{-1}}$ is 2.86 times greater than that at friction wind velocity of $u_* = 0.215\,\mathrm{m\,s^{-1}}$; while at the height of 0.2 m, the former is 176.32 times greater than the latter. Therefore, it is concluded that the significant increase of snow particles at the higher position is the major contributor to the increase of STR at higher wind speed mainly because the snow particles in the higher speed flow field can acquire more energy from the air and will rebound with a higher velocity.

Figure 8b shows the relationship of STR per unit area to the saltation height. As shown in Fig. 8b, the variations in the STR per unit area with height at different friction wind speeds are equivalent, that is, the STR per unit area decreases with height increasing. However, the STRs per unit area differ greatly at the same height at different friction wind speeds. In the same condition, the STRs per unit area at height $h = 0.01$ m under friction wind velocity of $u_* = 0.215$, 0.252, 0.288 and $0.361\,\mathrm{m\,s^{-1}}$ are 0.028, 0.057, 0.102 and $0.378\,\mathrm{kg\,m^{-2}\,s^{-1}}$, respectively.

TCD
9, 301–331, 2015

3.4 Velocity of snow particles

As one of the most important aspects to evaluate the accuracy of a drifting snow model, the velocity information of snow particles in the air is worthy of attention although it is seldom given in previous models. The location and velocity of every snow particle can be obtained, and the most important of all, the spanwise velocity of snow particles can be directly obtained in our simulation. The velocity distribution of snow particles in the air and the initial take-off velocity of the ejected particles are given in Sects. 3.4.1 and 3.4.2, respectively.

3.4.1 Velocity of snow particles in the air

The velocity distribution of snow particles in the air is shown in Fig. 9, in which (a) is the average velocity of snow particles along the streamwise direction as a function of height and (b) displays the corresponding velocity probability distribution of snow particles. It can be observed from Fig. 9a that the average velocity of snow particles along the streamwise direction increases with the height increasing and with the friction wind velocity at the same height increasing. It can be seen from Fig. 9b that the probability distribution of snow particles' velocity along the streamwise direction obeys the unimodal distribution. In other words, it distributes mainly at $0 \sim 3\,\mathrm{m\,s^{-1}}$ and the amount of snow particles moving in the opposite direction is less than 3 % of the total snow particles. Meanwhile, the probability distribution does not change with the friction wind speed, in agreement with our experiment. In this work, at friction wind velocity of $u_* = 0.288\,\mathrm{m\,s^{-1}}$, the proportions of snow particles with the velocity smaller than $1.5\,\mathrm{m\,s^{-1}}$ and greater than $4\,\mathrm{m\,s^{-1}}$ are 65.07 and 1.76 %, respectively, consistent with a field observation of Greeley et al. (1996) showing that the proportions of saltating particles with velocity smaller than $1.5\,\mathrm{m\,s^{-1}}$ and greater than $4\,\mathrm{m\,s^{-1}}$ are greater than 59 % and smaller than 3 %, respectively.

It should be noted that the high-speed particles in our simulation are significantly more than those captured in the experiments (Fig. 9b). This is mainly because the con-

TCD
9, 301–331, 2015

centration of snow particles decreases with height increasing, making it increasingly difficult to be captured the high-speed snow particles.

Figure 10 shows the spanwise velocity of snow particles in the air, where (a) is the distribution of the absolute value of spanwise velocity along the elevation and (b) is the corresponding probability distribution of snow particles' velocity. It is observed that the absolute value of spanwise velocity increases with height in an order of magnitude less than that of the streamwise velocity. The variation in the spanwise velocity with height at different friction wind velocity is not obvious.

From the above analysis it is quite evident that the velocity distribution of snow particles in the air is not sensitive to the wind velocity. The main reason for that is the wind velocity in the full development drifting snow slightly varies due to the reaction force of snow particles in the air.

3.4.2 Take-off velocity of snow particles

The initial take-off velocities of snow particles (including rebound particles) in a fully developed drifting snow field are presented in Fig. 11, in which the (a), (b), (c) and (d) show the distributions of streamwise, spanwise, vertical and resultant velocities, respectively. It is clear that all the velocity components obey the unimodal distribution and are not affected by the friction wind velocity.

Although there is no obvious difference in take-off velocity at different wind velocity, we can see that a large amount of particles may saltate at higher saltation height and greater friction wind speed. It may be inferred that turbulent fluctuation plays an important role in the lifting of snow particles.

3.5 Diameter distribution of snow particles in the air

The snow particles with mixed size close to natural situation are applied in our simulation. In this section, the size distribution of snow particles in the air is analyzed.

TCD
9, 301–331, 2015

Figure 12 shows the size distributions of snow particles in the air at different friction velocities, and their comparison with the experimental results. All the data have been normalized to the average of overall snow particles due to different characteristics of snow particles in different experiments. To avoid the random error, those data with snow particle influx less than $10^4\ m^{-2}\ s^{-1}$ have been eliminated. It is clearly that the mean diameter of snow particles near ground (with height below 0.05 m) is unchanged with the height increasing, which is consistent with the conclusion obtained by Gromke et al. (2014). However, the mean diameter of snow particles with height above 0.05 m exhibits a growing trend with height increasing, similar to the results observed by Sedmit (1984). This is mainly because larger particles withstand greater drag force in the air during the movement process and have higher impact velocity. Therefore, they will rebound with higher initial velocity because the rebound velocity is proportional to the incident velocity.

4 Conclusions

In this study, we establish a 3-D drifting snow model in the turbulent boundary layer, simulate the development process of drifting snow with mixed particle size and draw the following main conclusions:

1. Turbulent fluctuation may significantly affect the trajectory of small snow particles with equivalent diameter $d_p \leq 100\ \mu m$, while has little influence on that of particles with larger size.

2. The drifting snow in a turbulent boundary layer is very intermittent. Fully developed drifting snow swings forward toward the downwind in the form of snow streamers and the wind velocity is proportional to the concentration of snow particles at different locations of the turbulent boundary layer.

3. The velocities of snow particles along streamwise and spanwise directions increase with the height, and the latter is one order of magnitude less than the

TCD
9, 301–331, 2015

former in general. In addition, the velocity distribution is not sensitive to the wind speed.

4. The mean diameter of snow particles in the air is obviously distributed in layers. It is constant for snow particles with height less than 0.05 m, but shows a gradual increase trend for snow particles with height above 0.05 m.

Acknowledgements. This work is supported by the State Key Program of National Natural Science Foundation of China (91325203), the National Natural Science Foundation of China (11172118, 41371034), and the Innovative Research Groups of the National Natural Science Foundation of China (11121202), National Key Technologies R & D Program of China (2013BAC07B01).

References

Bavay, M., Lehning, M., Jonas, T., and Lowe, H.: Simulations of future snow cover and discharge in Alpine head water catchments, Hydrol. Process., 23, 95–108, 2009.

Bintanja, R.: Snowdrift suspension and atmospheric turbulence, Part I: Theoretical background and model description, Bound.-Lay. Meteorol., 95, 343–368, 2000a.

Bintanja, R.: Snowdrift suspension and atmospheric turbulence, Part II: Results of model simulations, Bound.-Lay. Meteorol., 95, 369–395, 2000b.

Clift, R., Grace, J. R., and Weber, M. E.: Bubbles, Drops and Particles, Academic Press, New York, 1978.

Déry, S. and Yau, M. K.: A bulk blowing snow model, Bound.-Lay. Meteorol., 93, 237–251, 1999.

Dupont, S., Bergametti, G., Marticorena, B., and Simoëns, S.: Modeling saltation intermittency, J. Geophys. Res., 118, 7109–7128, 2013.

Durán, O., Claudin, P., and Andreotti, B.: On aeolian transport: grain-scale interactions, dynamical mechanisms and scaling laws, Aeolian Res., 3, 243–270, 2011.

Fukushima, Y., Etoh, T., Ishiguro, S., Kosugi, K., and Sato, T.: Fluid dynamic analysis of snow drift using a non-Boussinesq k–ε turbulence model, Seppyo, 63, 373–383, 2001.

Fukushima, Y., Fujita, K., Suzuki, T., Kosugi, K., and Sato, T.: Flow analysis of developing snowdrifts using a k–ε turbulence model, Seppyo, 61, 285–296, 1999.

TCD
9, 301–331, 2015

Greeley, R., Blumberg, D. G., and Williams, S. H.: Field measurements of the flux and speed of wind-blown sand, Sedimentology, 43, 41–52, 1996.
Gromke, C., Horender, S., Walter, B., and Lehning, M.: Snow particle characteristics in the saltation layer, J. Glaciol., 60, 431–439, 2014.
Kok, J. F. and Renno, N. O.: A comprehensive numerical model of steady state saltation (COMSALT), J. Geophys. Res., 114, D17204, doi:10.1029/2009JD011702, 2009.
Lehning, M., Bartelt, P., Brown, B., and Fierz, C.: A physical SNOWPACK model for the Swiss avalanche warning, Part III: Meteorological forcing, thin layer formation and evaluation, Cold Reg. Sci. Technol., 35, 169–184, 2002.
Mann, G. W., Anderson, P. S., and Mobbs, S. D.: Profile measurements of blowing snow at Halley, Antarctica, J. Geophys. Res., 105, 24491–24508, 2000.
Michaux, J. L., Naaim-Bouvet, F., Kosugi, K., Sato, A., and Sato, T.: Study in a climatic wind tunnel (Cryospheric Environment Simulator) of the influence of the type of grain of snow and of the flow on the formation of a snow-drift, Houille Blanche, 6–7, 79–83, 2002.
Nemoto, M. and Nishimura, K.: Numerical simulation of snow saltation and suspension in a turbulent boundary layer, J. Geophys. Res., 109, D18206, doi:10.1029/2004JD004657, 2004.
Omiya, S., Sato, A., Kosugi, K., and Mochizuki, S.: Estimation of the electrostatic charge of individual blowing-snow particles by wind tunnel experiment, Ann. Glaciol., 52, 148–152, 2011.
Pomeroy, J. W., Gray, D. M., and Landine, P. G.: The prairie blowing snow model: characteristics, validation, operation, J. Hydrol., 144, 165–192, 1993.
Rice, M. A., Willetts, B. B., and McEwan, I. K.: An experimental study of multiple grain-size ejection produced by collisions of saltating grains with a flat bed, Sedimentology, 42, 695–706, 1995.
Schmidt, R. A.: Measuring particle size and snowfall intensity in drifting snow, Cold Reg. Sci. Technol., 9, 121–129, 1984.
Shao, Y. and Lu, H.: A simple expression for wind erosion threshold friction velocity, J. Geophys. Res., 105, 22437–22443, 2000.
Stout, J. E. and Zobeck, T. M.: Intermittent saltation, Sedimentology, 44, 959–970, 1997.
Taylor, P.: The thermodynamic effects of sublimating, blowing snow in the atmospheric boundary layer, Bound.-Lay. Meteorol., 89, 251–283, 1998.
Uematsu, T., Nakata, T., Takeuchi, K., Arisawa, Y., and Kaneda, Y.: Three-dimensional numerical simulation of snowdrift, Cold Reg. Sci. Technol., 20, 65–73, 1991.

TCD
9, 301–331, 2015

Vinkovic, I., Aguirre, C., Ayrault, M., and Simoëns, S.: Large-eddy simulation of the dispersion of solid particles in a turbulent boundary layer, Bound.-Lay. Meteorol., 121, 283–311, 2006.
Xiao, J., Bintanja, R., Déry, S., Mann, G., and Taylor, P.: An intercomparison among four models of blowing snow, Bound.-Lay. Meteorol., 97, 109–135, 2000.
Yamamoto, Y., Potthoff, M., Tanaka, T., Kajishima, T., and Tsuji, Y.: Large-eddy simulation of turbulent gas–particle flow in a vertical channel: effect of considering inter-particle collisions, J. Fluid Mech., 442, 303–334, 2001.
Zhang, J. and Huang, N.: Simulation of snow drift and the effects of snow particles on wind, Model. Simul. Eng., 2008, 408075–408076, 2008.
Zhou, Y. H., Li, W. Q., and Zheng, X. J.: Particle dynamics method simulations of stochastic collisions of sandy grain bed with mixed size in aeolian sand saltation, J. Geophys. Res., 111, D15108, doi:10.1029/2005JD006604, 2006.

TCD
9, 301–331, 2015

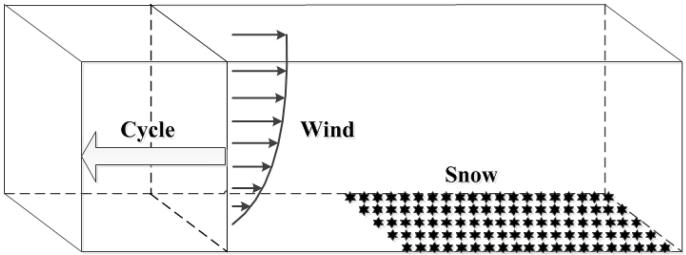

Figure 1. Diagram of computational region.

TCD
9, 301–331, 2015

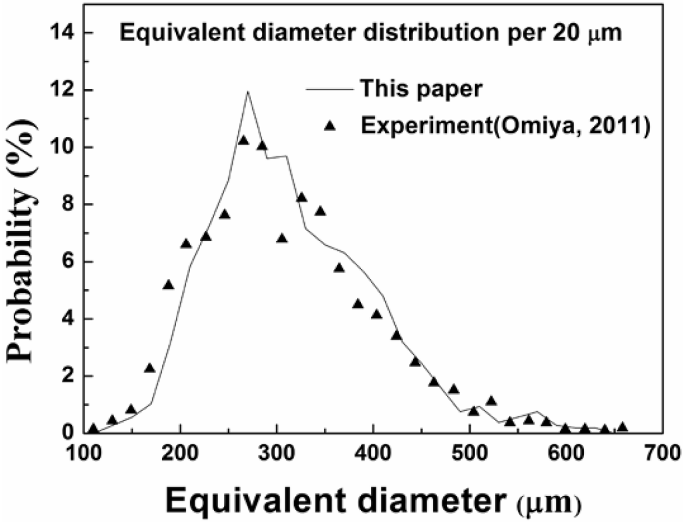

Figure 2. Equivalent diameter probability distribution of snow particles.

TCD
9, 301–331, 2015

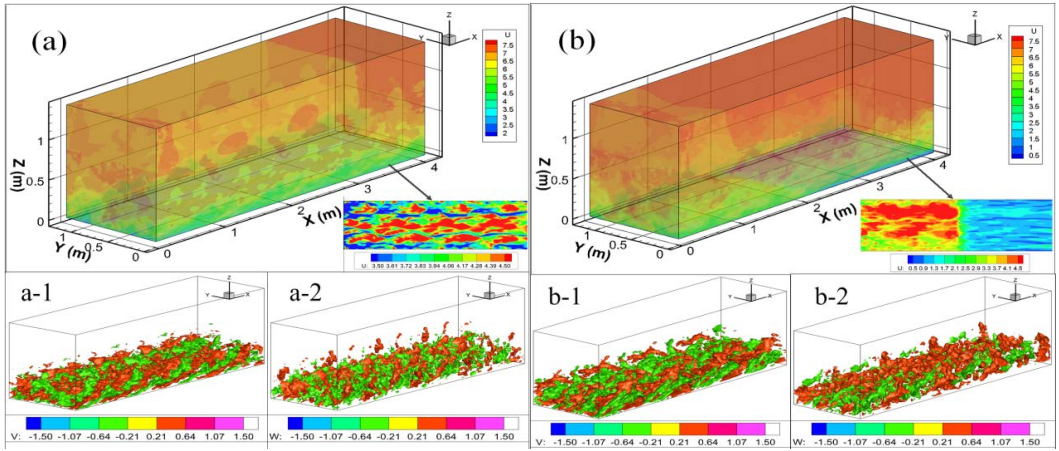

Figure 3. The cloud map of flow field at **(a)** t = 5 s and **(b)** t = 20 s.

TCD
9, 301–331, 2015

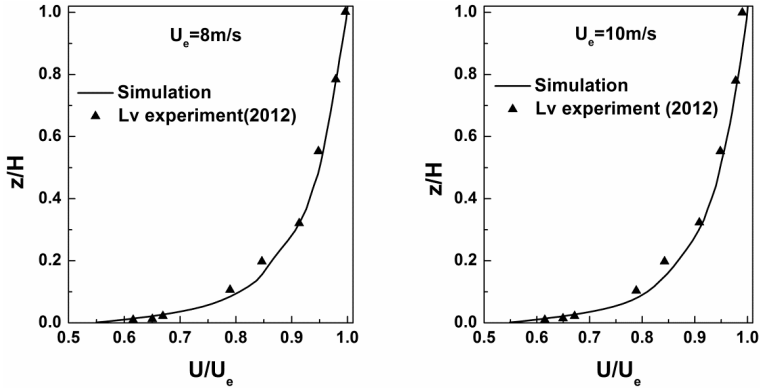

Figure 4. The wind profile at **(a)** $U_e = 8\,\mathrm{m\,s^{-1}}$ and **(b)** $U_e = 10\,\mathrm{m\,s^{-1}}$.

TCD
9, 301–331, 2015

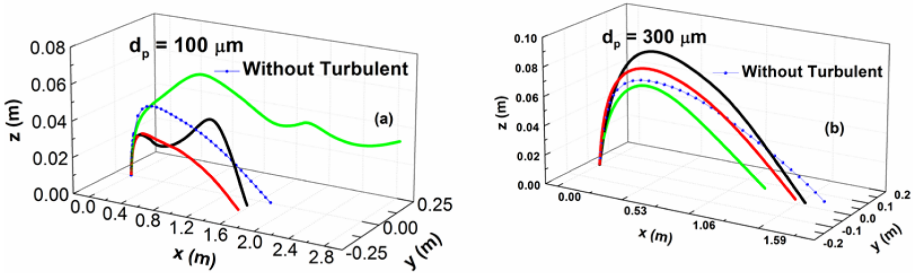

Figure 5. The 3-D trajectories of snow particles with different diameters ($u_* = 0.35\,\mathrm{m\,s^{-1}}$).

TCD
9, 301–331, 2015

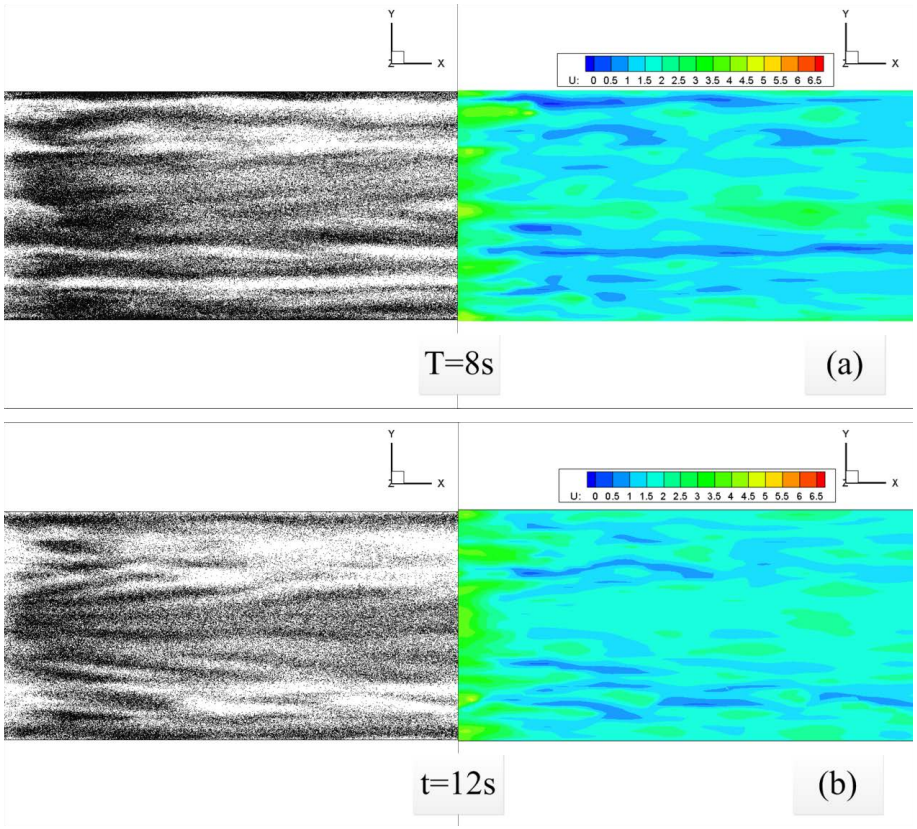

Figure 6. The top view of the particle concentration and the horizontal section of wind velocity cloud map at corresponding moment (U_e = 6.0 m s^{-1}, one dark spot stands for a snow particle and the height of horizontal section is H = 0.001 m).

TCD
9, 301–331, 2015

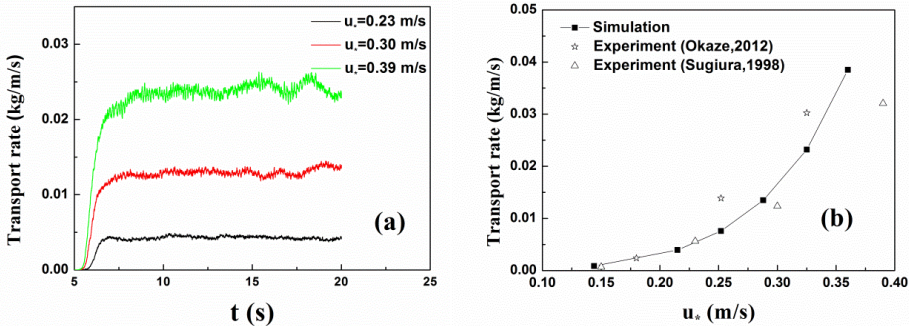

Figure 7. Variation of the snow transport rate (STR) per width with **(a)** time and **(b)** friction wind velocity.

TCD
9, 301–331, 2015

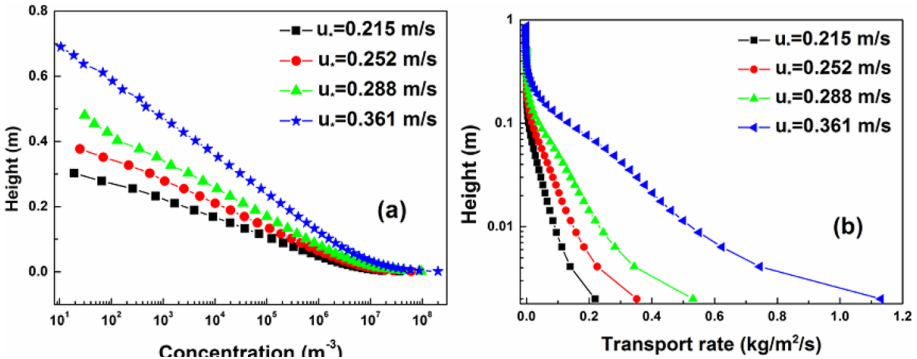

Figure 8. (a) The average particle concentrations and **(b)** STR per unit area vs. the height at different friction wind velocities.

TCD
9, 301–331, 2015

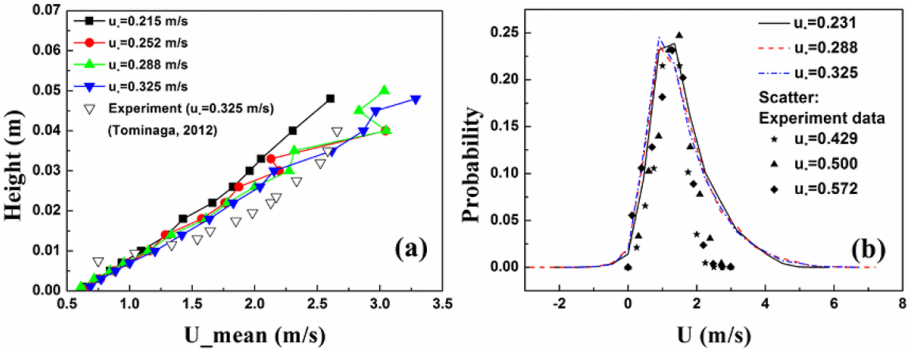

Figure 9. (a) Variation of the average velocity of snow particles along streamwise direction as a function of height and **(b)** the velocity probability distribution of snow particles.

TCD
9, 301–331, 2015

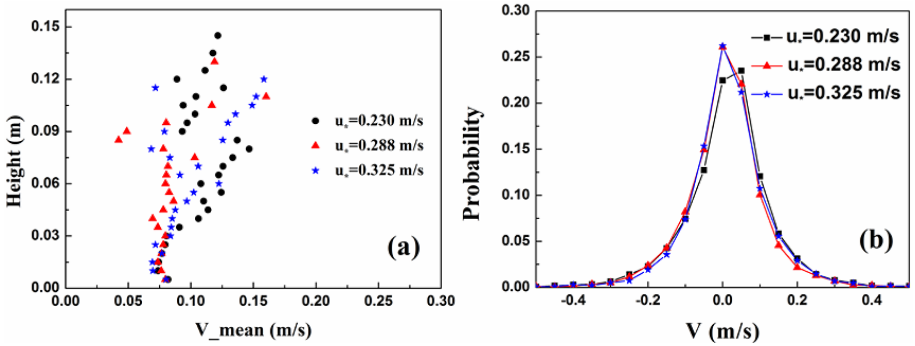

Figure 10. Distribution of **(a)** the absolute value of spanwise velocity along the elevation and **(b)** the corresponding probability distribution of snow particles in the air.

TCD
9, 301–331, 2015

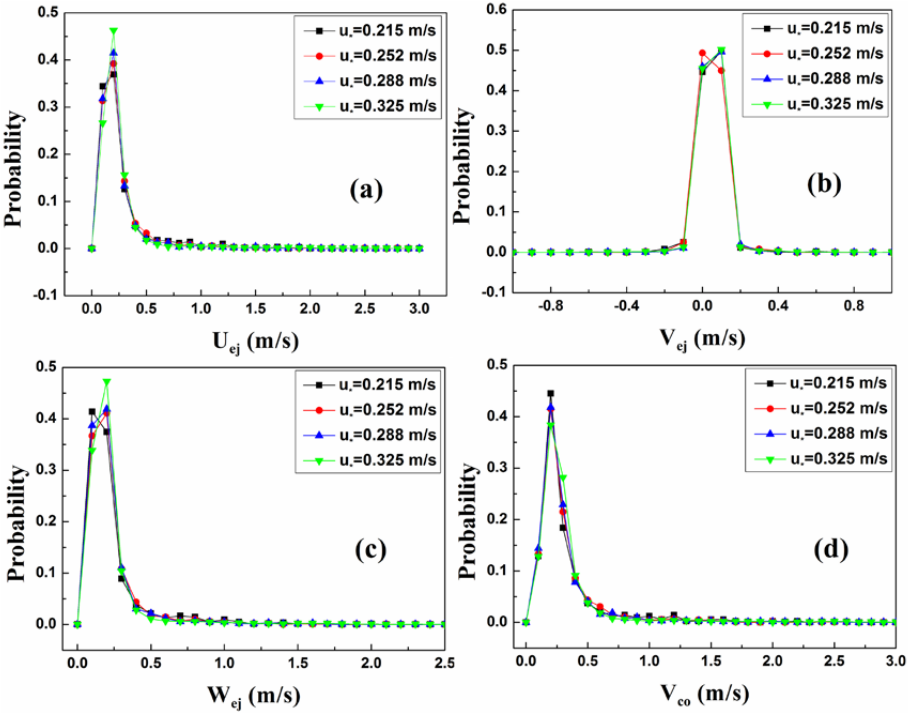

Figure 11. Distribution of the initial **(a)** streamwise, **(b)** spanwise, **(c)** vertical directions and **(d)** resultant take-off velocity of snow particles.

TCD
9, 301–331, 2015

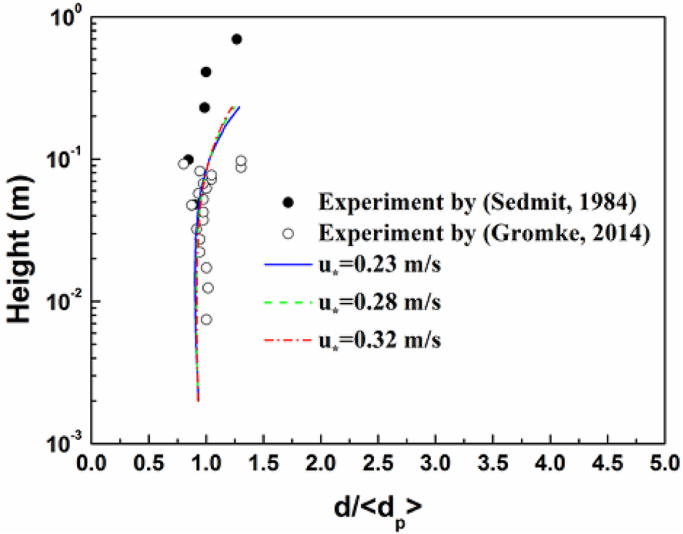

Figure 12. The mean equivalent diameter distribution of snow particles in the air vs. height.

TCD
9, 301–331, 2015